Putative reaction mechanism of nitrogenase after dissociation of a sulfide ligand

Cao, Lili; Ryde, Ulf

Published in:
Journal of Catalysis

DOI:
10.1016/j.jcat.2020.08.028

2020

Document Version:
Publisher's PDF, also known as Version of record

Journal of Catalysis 391 (2020) 247–259

Contents lists available at ScienceDirect

Journal of Catalysis

journal homepage: www.elsevier.com/locate/jcat

Putative reaction mechanism of nitrogenase after dissociation of a sulfide ligand

Lili Cao, Ulf Ryde *

Department of Theoretical Chemistry, Lund University, Chemical Centre, P.O. Box 124, SE-221 00 Lund, Sweden

ARTICLE INFO

Article history:
Received 4 February 2020
Revised 17 August 2020
Accepted 21 August 2020
Available online 1 September 2020

Keywords:
Nitrogenase
QM/MM
S2B dissociation
Nitrogen fixation
Alternating or distal reaction mechanism

ABSTRACT

We have investigated the implications of the recent crystallographic findings that the μ_2-bridging S2B sulfide ligand may reversibly dissociate from the active-site FeMo cluster of nitrogenase. We show with combined quantum mechanical and molecular mechanical (QM/MM) calculations that once S2B has dissociated, N_2 may bind in that position and can be protonated to two NH_3 groups by thermodynamically favourable steps. The substrate forms hydrogen bonds with two protein ligands, Gln-191 and His-195. For all steps, we have studied three possible protonation states of His-195 (protonated on either ND1, NE2 or both). We find that the thermodynamically favoured path involves an end-on NNH_2 structure, a mixed side-on/end-on H_2NNH structure, a side-on H_2NNH_2 structure, a bridging NH_2 structure and a bridging NH_3 structure. In all cases, His-195 seems to be protonated on the NE2 atom. Dissociation of the NH_3 product is often unfavourable and requires either further reduction or protonation of the cluster or rebinding of S2B. In conclusion, our calculations show that dissociation of S2B gives rise to a natural binding and reaction site for nitrogenase, between the Fe2 and Fe6 atoms, which can support an alternating reaction mechanism with favourable energetics.

1. Introduction

Nitrogenase (EC 1.18/19.6.1) is the only enzyme that can cleave the strong triple bond in N_2 [1–3]. This is one of the most important reaction in nature: Even if the atmosphere of earth contains 78% N_2, nitrogen is typically a limiting element for plant growth and a major component of artificial fertilizers. The reason for this is that the triple bond in N_2 is very strong, making the molecule inert [3,4].

The nitrogenase reaction is demanding, requiring 16 molecules of ATP, eight electrons and eight protons to cleave one N≡N triple bond: [1–3]

$$N_2 + 8e^- + 8H^+ + 16ATP \rightarrow 2NH_3 + H_2 + 16ADP + 16P_i \quad (1)$$

Nitrogenase is a large and complicated system [1–3,5–9]. It consists of two components. The Fe protein contains a Fe_4S_4 cluster and binds two molecules of ATP. In the ATP-loaded state, it docks to the MoFe protein and delivers electrons to the active-site FeMo cluster, via a $Fe_8S_7Cys_6$ site, called the P-cluster. After hydrolysis of the ATP molecules, the Fe protein is released and a new reduced and ATP-loaded Fe-protein may bind. The active site consists of a $MoFe_7S_9C$(homocitrate)CysHis cluster, [5–9] although alternative nitrogenases exist, in which the Mo ion is replaced by V or Fe [10].

Nitrogenase has been thoroughly studied with biochemical, kinetic, crystallographic and spectroscopic methods [1–3,11–16]. The reaction is often described by nine intermediates, E_0–E_8, differing in the number of added electrons and protons, the Lowe–Thorneley cycle [17]. It is currently believed that four electrons have to be added before N_2 can bind and that H_2 formation through reductive elimination is a prerequisite for the binding [1]. It is also believed that Fe2 and Fe6 are involved in the binding of N_2 (the numbering of the Fe ions is shown in Fig. 1a) [3].

Many density-functional theory (DFT) studies have been performed to study the reaction mechanism of nitrogenase, but no consensus has been reached so far [3,12,18–32]. For example, it has been much disputed whether N_2 is protonated first by three protons on one of the N atoms, which leaves as NH_3 at the E_5 stage, before the second N atom is protonated, or if the protons are added alternatively to both N atoms, so that HNNH and H_2NNH_2 are intermediates and the first NH_3 molecule does not dissociate until the E_7 stage [3,33]. These two mechanisms are called the distal and alternating pathways, respectively, and they are illustrated in Fig. 2. The distal pathway was originally suggested by Chatt and has gained support from inorganic model complexes [34–38].

* Corresponding author.
E-mail address: Ulf.Ryde@teokem.lu.se (U. Ryde).

https://doi.org/10.1016/j.jcat.2020.08.028
0021-9517/

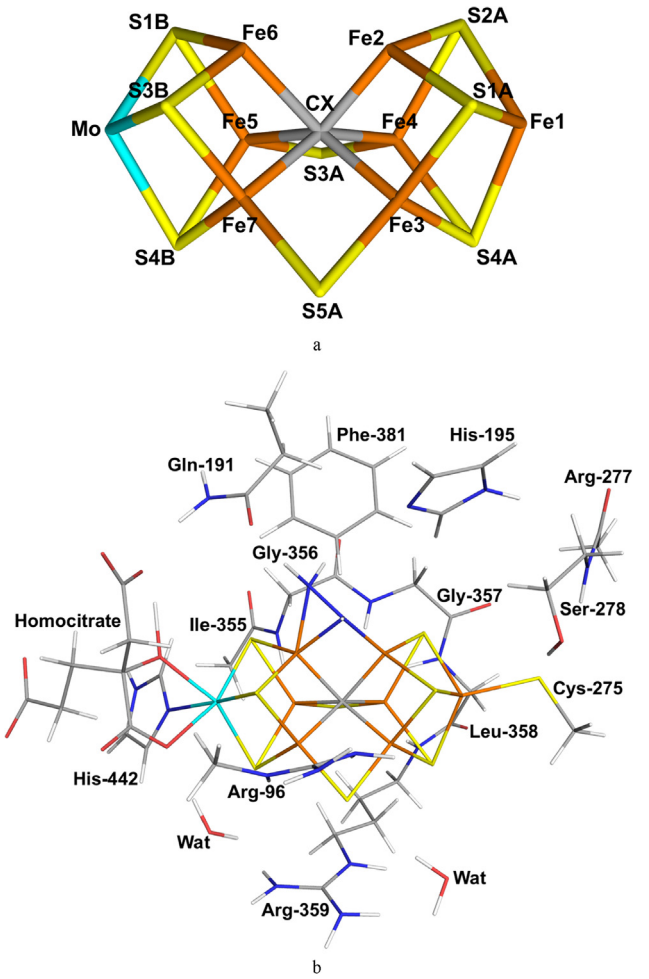

Fig. 1. a) The Mo-nitrogenase FeMo cluster with S2B dissociated (it was bridging Fe2 and Fe6 before dissociation) and atom names from the 3U7Q crystal structure [7]. b) The QM system used in the QM/MM calculations (with H_2NNH bound).

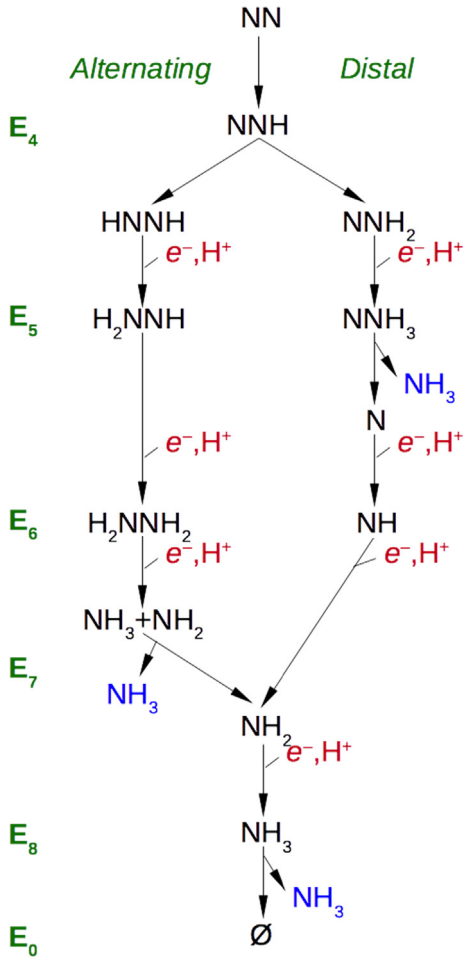

Fig. 2. The alternating and distal pathways suggested for the second part (E_4–E_8) of the nitrogenase mechanism, [3,33] showing the N_2-derived intermediates.

However, it has been suggested to apply also for nitrogenase by several authors [20,39]. The alternating pathway is supported by the fact that nitrogenase can use hydrazine as a substrate and that hydrazine is released upon acid or base hydrolysis of the enzyme during turnover [1,3,40,41]. Moreover, it has been shown that N_2, N_2H_2, CH_3N_2H and N_2H_4 all react via common intermediate, which strongly supports an alternative mechanism [3,33].

Most studies have assumed that the FeMo cluster remains intact throughout the reaction. However, in 2014, Rees et al. published a crystal structure of CO-inhibited Mo-nitrogenase, in which CO replaces one of the sulfide ions (S2B, bridging the Fe2 and Fe6 ions; cf. Fig. 1a) of the FeMo cluster and binds to the Fe2 and Fe6 atoms [8]. They suggested that something similar might happen during the normal reaction mechanism of the enzyme, i.e. that the S2B ligand is labile and may dissociate reversibly during the reaction, forming a binding site for the N_2 substrate. This was recently supported by another crystal structure of V-nitrogenase, in which S2B had also dissociated from the cluster [39]. In that structure, the nearby Gln-176 had changed its position, forming a pocket close to the active site, in which they found a prominent density, assigned to a HS^- ion. This indicates that S2B may be protonated and displaced from the active site, but kept stored nearby inside the protein so that it can easily bind back again. Moreover, they found a light atom bound to the FeV cluster at the former position of S2B. They interpreted it as a nitrogen atom, which could represent the E_6 or E_7 intermediate (formally NH^{2-} or NH_2^-) of a distal reaction mechanism. Yet, Bjornsson and coworkers showed by a combined quantum mechanics and molecular mechanics (QM/MM) study that the crystal structure most likely contains a OH^- ligand, rather than a N_2-derived group, [42] although this study has not convinced the crystallographers [39].

However, even if the crystal structure involves OH^-, it is still possible that S2B reversibly dissociates from the cluster during the reaction mechanism and N_2 binds to that site. In fact, Nørskov et al. suggested such a mechanism for Mo-nitrogenase in 2015, based on QM-cluster calculations [20]. In their mechanism, N_2 binds end-on to both Fe2 and Fe6 and is then sequentially protonated along a distal pathway. However, these calculations involved a oversimplified model of the cluster (with histidine modelled by NH_3 and homocitrate by two OH^- ions), no parts of the surrounding enzyme were included and it was assumed that the E_0 state is doubly protonated, which recent quantum-refinement calculations have shown not to be the case [43].

Therefore, we here provide a more detailed study of the reaction mechanism of Mo-nitrogenase, assuming that the S2B group dissociates from the FeMo cluster and N_2 binds in its position. Our calculations employ QM/MM methods, including the entire solvated heterotetrameric structure of nitrogenase in the calculations. We thoroughly investigate the energetics and electronic structure of possible intermediates of both the alternating and distal mechanism and also different protonation states of His-195, which can form hydrogen bonds to the N_2-derived ligand. Even if there is no conclusive evidence that dissociation of S2B is involved in the

catalytic mechanism of nitrogenase, this study provides structures and energies for such a mechanism that can be compared to experiments and to similar studies of the reaction without dissociation of S2B.

2. Methods

2.1. The protein

The QM/MM calculations were based on the 1.0-Å crystal structure of Mo-nitrogenase from *Azotobacter vinelandii* (PDB code 3U7Q) [7]. The setup of the protein is identical to that of our previous studies of the protein [44–48]. The entire heterotetramer was included in the calculations, because the various subunits are entangled without any natural way to separate them. The QM calculations were concentrated on the FeMo clusters in the C subunit because there is a buried imidazole molecule from the solvent rather close to the active site (~11 Å) in the A subunit. The two P clusters and the FeMo cluster in subunit A were modelled by MM in the fully reduced and resting states, respectively [44].

The protonation states of all residues were the same as before [44]: All Arg, Lys, Asp and Glu residues were assumed to be charged, except Glu-153, 440 and 231D (a letter "D" after the residue number indicates that it belongs to that subunit; if no letter is given, it belongs to subunit C; subunits A and B are identical to the C and D residues). Cys residues coordinating to Fe ions were assumed to be deprotonated. His-274, 451, 297D, 359D and 519D were assumed to be protonated on the ND1 atom, His-31, 196, 285, 383, 90D, 185D, 363D and 457D were presumed to be protonated on both the ND1 and NE2 atoms (and therefore positively charged), whereas the remaining 14 His residues were modelled with a proton on the NE2 atom. The homocitrate ligand was modelled in the singly protonated state with a proton shared between the hydroxyl group (which coordinates to Mo) and the O1 carboxylate atom. This protonation state was found to be the most stable one in an extensive QM/MM, molecular dynamics and quantum-refinement study [44] and this protonation state is also supported by another recent study [49].

The protein was solvated in a sphere with a radius of 65 Å around the geometrical centre of the protein. 160 Cl^- and 182 Na^+ ions were added at random positions (but not inside the protein [44]) to neutralise the protein and give an ionic strength of 0.2 M [50]. The final system contained 133 915 atoms. The added protons, counter ions and water molecules were optimised by a simulated annealing calculation (up to 370 K), followed by a minimisation, keeping the other atoms fixed at the crystal-structure positions [44].

All MM calculations were performed with the Amber software [51]. For the protein, we used the Amber ff14SB force field [52] and water molecules were described by the TIP3P model [53]. For the metal sites, the MM parameters were the same as in our previous investigation [44]. The metal sites [44,48] were treated by a non-bonded model [54] and charges were obtained with the restrained electrostatic potential method, obtained at the TPSS/def2-SV(P) level of theory [55,56] and sampled with the Merz–Kollman scheme [57].

The FeMo cluster was modelled by $MoFe_7S_8C$(homocitrate)(CH_3S)(imidazole), where the two last groups are models of Cys-275 and His-442. In addition, all groups that form hydrogen bonds to the FeMo cluster were also included in the QM system, viz. Arg-96 and His-195 (sidechains), Ser-278 and Arg-359 (both backbone and sidechain, including the Cα and C and O atoms from Arg-277), Gly-356, Gly-357 and Leu-358 (backbone, including the Cα and C and O atoms from Ile-355), as well as two water molecules. Following the crystal structure of V-nitrogenase with the putative N-intermediate, [39] S2B was removed from the FeMo cluster. Moreover, the sidechain of Gln-191 was included in the QM system and this group was flipped so that OE1 points towards the former position of S2B and His-195, whereas the NE2 atom of Gln-191 still forms a hydrogen bond to one of the carboxylate groups of the homocitrate ligand (1.8–1.9 Å H···O distance). Finally, Phe-381 was also included, because it is close to the putative N_2 binding site. The QM system involved 170–178 atoms in total (depending on the number of added protons and N atoms) and is shown in Fig. 1b. The charge was −1, except in a few cases when electrons and protons were not added together.

2.2. QM calculations

All QM calculations were performed with the Turbomole software (versions 7.1 and 7.2) [58]. We employed two DFT methods, TPSS [55] and B3LYP [59–61], and the def2-SV(P) basis set [56] (previous calculations on nitrogenase have shown that larger basis sets has only a small influence on the energies, less than 15 kJ/mol [44–48]). The calculations were sped up by expanding the Coulomb interactions in an auxiliary basis set, the resolution-of-identity (RI) approximation [62,63]. Empirical dispersion corrections were included with the DFT-D3 approach [64] and Becke–Johnson damping [65], as implemented in Turbomole.

Experiments have shown that the ground spin state of E_0 and E_2 are quartets with a surplus of three α electrons, whereas E_4 is a doublet [3,12]. Consequently, we used these spin states for these three states. For the other oxidation states, we checked which of the two or three lowest spin states has the most favourable energy at the TPSS and B3LYP/def2-SV(P) levels of theory.

The electronic structure of all QM calculations was obtained with the broken-symmetry (BS) approach [30]: Each of the seven Fe ions were modelled in the high-spin state, with either a surplus of α (four Fe ions) or β (three Fe ions) spin. Such a state can be selected in 35 different ways ($\frac{7!}{3!4!}$) [45]. A starting wavefunction was obtained by first optimising the all-high-spin state with 35 unpaired electrons and then changing the total α and β occupation numbers to the desired net spin. This gave one of the BS states. The other BS states were obtained by simply swapping the coordinates of the Fe ions [66]. In some cases, we instead used the fragment approach by Szilagyi and Winslow to obtain a proper BS state [67]. The various BS states are named by listing the number in the Noodleman nomenclature (BS1–10) [30], followed by the numbers of the three Fe ions with minority spin, e.g. BS7-235, indicating that Fe2, Fe3 and Fe5 have β spin. For ligand-bound structures, previous studies have shown that the spin on some Fe ions is often quite low and sometimes states with only two Fe β spin might become competitive [46]. Such states were also considered and they are named by just giving the two Fe ions with negative spin, e.g. BS-14, indicating that Fe1 and Fe4 have β spin. We have thoroughly studied the 35 BS states for the resting state, the protonated resting state and the reduced state, and how their energies vary with the QM method, the size of the basis set, the geometry and the influence of the surroundings [45]. For each E_n state, we studied the relative energy of all BS states with both TPSS and B3LYP/def2-SV(P).

As have been discussed before [45,47], TPSS-D3/def2-SV(P) calculations give geometries that reproduce the crystal structure of the resting state of nitrogenase excellently with average and maximum deviations of 0.05 and 0.09 Å for the metal–metal and 0.02 and 0.06 Å metal–ligand distances, respectively and a root-mean-squared-deviation (RMSD) of 0.06 Å for the metals and the first-sphere ligands. This is similar to the results obtained with the TPSSh approach [49] and appreciably better than with the B3LYP-D3/def2-SV(P) method, which gives average and maximum

deviations of 0.08 and 0.12 Å for the metal–metal and 0.04 and 0.11 Å metal–ligand distances, respectively and a RMSD of 0.08 Å. Therefore, we discuss primarily the TPSS-D3/def2-SV(P) results.

2.3. QM/MM calculations

The QM/MM calculations were performed with the COMQUM software [68,69]. In this approach, the protein and solvent are split into two subsystems: System 1 (the QM region) was relaxed by QM methods. System 2 contained the remaining part of the protein and the solvent and it was kept fixed at the original coordinates (equilibrated crystal structure to avoid the risk that different calculations end up in different local minima). The total system was spherical and non-periodic with 133 915 atoms.

In the QM calculations, system 1 was represented by a wavefunction, whereas all the other atoms were represented by an array of partial point charges, one for each atom, taken from the MM setup. Thereby, the polarisation of the QM system by the surroundings is included in a self-consistent manner (electrostatic embedding). When there is a bond between systems 1 and 2 (a junction), the hydrogen link-atom approach was employed: The QM system was capped with hydrogen atoms (hydrogen link atoms, HL), the positions of which are linearly related to the corresponding carbon atoms (carbon link atoms, CL) in the full system [68,70]. All atoms were included in the point-charge model, except the CL atoms [71].

The total QM/MM energy in ComQum was calculated as [68,69]

$$E_{\mathrm{QM/MM}} = E^{\mathrm{HL}}_{\mathrm{QM1+ptch2}} + E^{\mathrm{CL}}_{\mathrm{MM12},q_1=0} - E^{\mathrm{HL}}_{\mathrm{MM1},q_1=0} \quad (2)$$

where $E^{\mathrm{HL}}_{\mathrm{QM1+ptch2}}$ is the QM energy of the QM system truncated by HL atoms and embedded in the set of point charges modelling system 2 (but excluding the self-energy of the point charges). $E^{\mathrm{HL}}_{\mathrm{MM1},q_1=0}$ is the MM energy of the QM system, still truncated by HL atoms, but without any electrostatic interactions. Finally, $E^{\mathrm{CL}}_{\mathrm{MM12},q1=0}$ is the classical energy of all atoms in the system with CL atoms and with the charges of the QM region set to zero (to avoid double-counting of the electrostatic interactions). Thus, ComQum employs a subtractive scheme with electrostatic embedding and van der Waals link-atom corrections [72]. No cutoff is used for any of the interactions in the three energy terms in Eqn. 3.

The geometry optimisations were continued until the energy change between two iterations was less than 2.6 J/mol (10^{-6} a.u.) and the maximum norm of the Cartesian gradients was below 10^{-3} a.u.

3. Result and discussion

Inspired by the recent crystal structures of Mo and V-nitrogenase, showing that the S2B sulfide group may dissociate reversibly from the active site [8,39], we investigate whether N_2 may bind to the empty position between Fe2 and Fe6 ions, previously occupied by S2B, and react to form two molecules of NH_3. Since the great majority of previous QM studies of nitrogenase have been performed on the Mo enzyme [3,12,18–24,26–32], we decided to study that enzyme. Therefore, we removed the S2B ligand from the FeMo cluster and replaced it with N_2 in the bridging position between Fe2 and Fe6. Moreover, we flipped the Gln-191 residue in the same way as observed for Gln-176 in the crystal structure of V-nitrogenase, i.e. so that the OE1 atom points towards N_2 and His-195 (corresponding to His-180 in V-nitrogenase), whereas the NE2 atom still forms a hydrogen bond to the acetate group of the homocitrate ligand (cf. Fig. 1b).

Dissociation of S2B opens a natural binding site for N_2, which strongly facilitates the computational modelling of the reaction mechanism (in a previous study, we investigated ~ 60 different binding modes, assuming that S2B remains bound [48]). Moreover, it avoids the problem of defining the E_4 state before H_2 dissociation and N_2 binding, for which there are even more possibilities and for which there has been strong disagreement between various computational studies [14,21,43,47,73–76]. On the other hand, the protonation of His-195, which is within hydrogen-bonding distance to the substrate, can be expected to strongly affect the results. Therefore, we investigated the three possible protonation states of this residue, viz. singly protonated on either the ND1 or NE2 atoms, or protonated on both atoms. These states are called HID, HIE and HIP in the following.

As mentioned in the introduction, the nitrogenase mechanism is normally described by the nine E_0–E_8 states in the Lowe–Thorneley cycle [17]. E_0 is the resting state, which is in the $Mo^{III}Fe^{II}_3Fe^{III}_4$ oxidation state [12,21,49,77]. In this study, we have considered the E_4–E_8 states, after the dissociation of H_2 and binding of N_2. To clarify exactly what state has been studied, we will use a more detailed nomenclature. We denote each state by $e_ih_jn_k$, where i is the number of extra electrons, j is the number of extra protons and k is the number of extra nitrogen atoms relative to a E_0 resting state with S2B dissociated (i.e. $MoFe_7S_8C$ in the $Mo^{III}Fe^{II}_3Fe^{III}_4$ oxidation state, without any bound hydrogen atoms). The starting, N_2-bound E_4 state is then $e_2h_2n_2$, because four electrons and protons have been added, but two of each have dissociated again with H_2. We then add successively four more electrons and protons, and investigate where these preferably go, when the N–N bond is cleaved and when NH_3 dissociates (taking three electrons, three protons and one nitrogen with it).

We try to determine the most stable conformation of the E_4–E_8 states (i.e. protonation and binding mode of the N_2-derived intermediate). Thereby, we get information whether a reaction mechanism of Mo-nitrogenase with a dissociated S2B group is thermodynamically feasible and whether it follows a distal or alternating mechanism (cf. Fig. 2).

3.1. N_2-bound E_4 structures, $e_2h_2n_2$

We start with the N_2-bond E_4 state of the protein. To avoid speculating about the structure of the E_4 or E_2states of the FeMo cluster, for which there are many possible protonation and electronic states, and for which there is still no consensus about the structure, [3,13,14,21,32,43,46,74–76,78,79] because different DFT functionals give widely different results [47], we first assume that the two added protons have bound to N_2, forming either HNNH or NNH_2 [48].

Thus, we started to optimise with QM/MM the structure of *cis*-HNNH bound side-on to Fe2 and Fe6 (with His-195 in the HIE state). The structure is shown in Fig. 3 (under HNNH). The two Fe–N distances are quite similar, 1.80 and 1.88 Å, as can be seen in Table 1. The N–N bond length is 1.29 Å, which is slightly longer than in free *cis*-HNNH (1.24 Å), optimised at the same QM level of theory. The structure is stabilised by a short hydrogen bond from HNNH to the carbonyl oxygen of Gln-191 (the H···O distance is 1.49 Å). The other proton of HNNH points against the NE2 atom of His-195 (2.18 Å), but this atom is already protonated so the interaction is probably not very favourable. The BS investigation of this structure, presented in Table S2, showed that it is most stable in the BS8-345 state. It has a low spin population on Fe6 (0.5), whereas that on Fe2 (2.7) is similar to that on the other Fe ions (2.3–2.7, in absolute terms), except that on Fe1 (3.3). The Mo ion has a low spin population (–0.1).

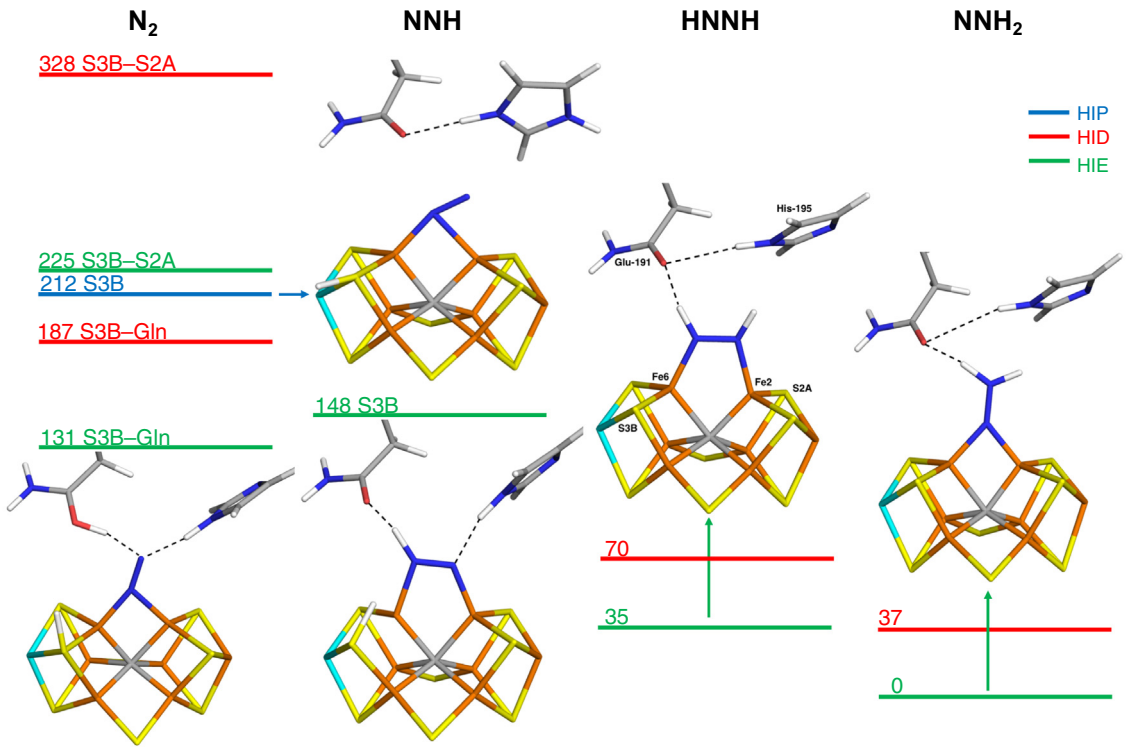

Fig. 3. The QM/MM geometries and TPSS/def2-SV(P) energies (kJ/mol) of the N_2-bound E_4 structures with N_2, NNH, HNNH and NNH_2. Hydrogen bonds are shown by dashed lines.

The corresponding HID structure has similar N–N and Fe–N bond lengths (1.28, 1.90 and 1.83 Å) and a similar strong hydrogen bond to Gln-191 (1.46 Å), but the hydrogen bond to His-195 is appreciably stronger (1.73 Å) because the NE2 atom is now not protonated. However, this HID structure is 35 kJ/mol less stable than the corresponding HIE structure (but only 3 kJ/mol with B3LYP), reflecting that the HIE structure is intrinsically more stable (e.g. by 41 kJ/mol for the E_0 state; 39 kJ/mol with B3LYP).

Fig. 3 also shows the structure of NNH_2 bound end-on to nitrogenase with His-195 in the HIE state. The unprotonated N atom interacts symmetrically with both Fe2 and Fe6 (the Fe–N bonds are 1.79 and 1.80 Å). The N–N bond is 1.27 Å, i.e. slightly longer than for free NNH_2 (1.21 Å). This structure is also stabilised by a strong hydrogen bond to the carbonyl oxygen of Gln-191 (1.48 Å), whereas the other proton points towards His-195 (2.19 Å), without making any favourable interaction. It turned out to be most stable in the BS10-147 state (Table S2; BS10-135 with B3LYP). It has low and negative spin populations on both Fe2 and Fe6 (–1.5 and –1.6), whereas the other Fe ions have larger spin populations (3.1 on Fe1 and 2.6–2.9 on the other ions). The spin on Mo is small but positive (0.2). Interestingly, this structure turned out to be 35 kJ/mol more stable than the side-on HNNH structure (31 kJ/mol with the best B3LYP states), although isolated NNH_2 is 64 kJ/mol less stable than *cis*-HNNH at the same level of theory (61–73 kJ/mol with different DFT functionals, basis sets and with or without a water-like continuum solvent). This agrees with the structure suggested by Nørskov and coworkers [20]. The corresponding HID structure is similar (Table 1), but has a hydrogen bond between NE2 of His-195 and the second hydrogen on NNH_2 (1.64 Å). It is 37 kJ/mol less stable than the HIE structure.

To put these structures in a perspective, we also performed some investigations of the corresponding N_2-bound structures (although far from exhaustive regarding possible positions of the two protons). An example with the two protons on S3B and His-195 (i.e. a HIP structure) is shown in Fig. 3, showing that N_2 is asymmetrically bound to Fe2 and Fe6. One N atom is 1.80 Å from Fe6 and 2.02 Å from Fe2, whereas the other is 2.10 Å from Fe2. The N–N distance is 1.17 Å, i.e. 0.06 Å longer than for free N_2 optimised at the same level of theory. N_2 is not stabilised by any hydrogen bonds. Instead, the doubly protonated His-195 forms a hydrogen bond with Gln-191 (2.01 Å). In this structure, Fe6 has a low spin population (2.0), whereas that on Fe2 (2.7) is similar to that of the other Fe ions (2.7–3.0, but 3.2 on Fe1). This structure is 212 kJ/mol less stable than the NNH_2 structure (117 kJ/mol with B3LYP), showing that protonation of the substrate is strongly favourable.

A structure with His-195 in the HIE state and S2A protonated instead is slightly less stable (13 kJ/mol), whereas the corresponding HID structure is strongly unfavourable (by 116 kJ/mol). However, a more stable N_2 structure was unexpectedly found if the OE1 atom of Gln-191 was protonated. As can be seen in Fig. 3, it is stabilised by hydrogen bonds from both Gln-191 and His-195 to the distal atom of N_2. It has Fe–N bonds of 1.78 (Fe6) and 2.00 (Fe2) Å and a slightly longer N–N bond, 1.18 Å. It is actually 81 kJ/mol more stable than the structure protonated on His-195, but still 131 kJ/mol less stable than the NNH_2 structure (49 kJ/mol with B3LYP).

We also studied some structures with NNH bound to the cluster. An example with S3B protonated and His-195 in the HIE state is shown in Fig. 3. NNH binds side-on to the two Fe ions with Fe–N bonds lengths of 1.84 and 1.88 Å and a N–N bond of 1.24 Å. The protonated N atom (coordinated to Fe6) forms a strong hydrogen bond to OE1 of Gln-191 (1.30 Å), whereas the other N atom receives a hydrogen bond from His-195 (1.93 Å). This structure is 17 kJ/mol less stable than the best N_2 structure (with Gln-191 protonated; 36 kJ/mol with B3LYP) and 148 kJ/mol less stable than the best N_2H_2 structure (85 kJ/mol with B3LYP). In the corresponding HID structure, the proton on NNH is spontaneously transferred to Gln-191, giving rise to the N_2–S3B–Gln structure.

Table 1
Energies (TPSS-D3/def2-SV(P) and B3LYP-D3/def2-SV(P) energies in kJ/mol) and geometries (Å) of the various structures. The N–N and N–Fe bond lengths are given, together with possible hydrogen bond lengths to OE1 of Gln-191 (NH···OE1) and to NE2 or HE2 of His-195 (NH···NE2 or N···HE2). The last column (Q–H) gives the hydrogen-bond distance between OE1 of Gln-191 and HE2 of His-195.

Structure	His	*S*	BS	Energy		N–N	N1		N2		Gln	His	Q-H
				TP	B3		Fe2	Fe6	Fe2	Fe6			
e2h2n2													
N_2-S3B-S2A	HID	½	BS10-135	328	204	1.16	2.09	1.87	2.10				
	HIE		BS10-135	225	115	1.16	2.05	1.84	2.08			2.34	2.44
N_2-S3B-HIP	HIP		BS10-135	212	117	1.17	2.02	1.80	2.10				2.01
N_2-S3B-Gln	HID		BS10-135	187	84	1.16	2.05	1.79			1.78[a]		3.05
	HIE		BS10-135	131	49	1.18	2.00	1.78			1.59[a]	1.79	
NNH-S3B	HIE		BS10-135	148	85	1.24	1.84		1.88		1.30	1.93	
NNH_2	HID		BS10-147	37	54	1.26	1.82	1.81			1.45	1.64	
	HIE		BS10-147	0	49	1.27	1.79	1.80			1.48	2.19	2.75
			BS10-135	2	0	1.27	1.79	1.80			1.48	2.18	2.78
HNNH	HID		BS10-135	70	34	1.28	1.90			1.83	1.46	1.73	
	HIE		BS8-345	35	31	1.29	1.80			1.88	1.49	2.18	2.36
e3h3n2													
HNNH	HIP	1	BS7-235	137	126	1.32	1.92			1.77	1.71	2.50	1.85
$HNNH_2$	HID	1	BS10-135	47	107	1.39	2.00		1.89	1.88	1.70	1.68	1.68
	HIE	1	BS7-247	53	22	1.41	1.98		2.47	1.78	1.58	2.39	2.32
H_2NNH	HID	1	BS7-235	39	55	1.39		1.96	1.92	1.92	1.53		
	HIE	1	BS7-247	0	0	1.40		1.93	1.95	2.00	1.54	2.62	
NNH_2	HIP	2	BS7-247	71	**72**	1.39	1.79	1.81			1.37	1.68	
NNH_3	HID	1	BS7-247	51	34	1.40	1.82	1.77			1.46	1.66	
	HIE	2	BS7-247	83	78	1.40	1.78	1.81			1.38	2.19	2.84
		1	BS7-235	88	64	1.40	1.79	1.75			1.34	2.14	2.92
e4h4n2													
H_2NNH	HIP	½	BS7-346	139	189	1.45		1.97	1.91		1.58		1.93
$HNNH_2$	HIP		BS7-346	180	233	1.41	2.50	1.82	1.96		1.73	2.64	1.64
H_2NNH_2	HID		BS7-346	35	83	1.44		1.97	1.98		1.50	1.72	
	HIE		BS10-135	0	55	1.45		1.96	1.98		1.54	2.34	2.24
			BS8-345	5	0	1.45		1.96	2.02		1.52	2.30	2.21
NNH_3	HIP		BS10-147	250	315	1.40	1.83	1.81			1.43	2.08	
$HNNH_3$	HID		BS10-147	13	78	1.44	1.94	1.92			1.45	1.64	
	HIE		BS10-147	46	114	1.45	1.91	1.91			1.40	2.16	2.76
NH_4 + N	HID		BS10-147	77			1.69	1.73			1.62	1.62	
e5h5n2													
H_2NNH_2	HIP	0	BS10-135	297	315	1.45		1.96	2.00		1.67		1.94
H_2NNH_3	HID	0	BS10-135	294	320	1.46		1.99			1.63	1.56	
NH_2 + NH_3	HID	1	BS7-235	101	101		1.99	1.85	2.07		1.66	2.09	
	HIE	0	BS10-135	0	67		1.96	1.87	2.05		1.71	2.46	2.15
		1	BS7-235	4	0		1.99	1.87	2.10		1.71		2.16
NH_3 + NH_2	HIE	0	BS10-135	23				1.88	2.03	2.01	1.58		2.28
			BS10-135	100	173			1.97	1.88		1.83		3.16
e0n1													
N	HID	2	BS-15	86	85		1.71	1.69					
	HIE		BS-15	0	0		1.70	1.70				2.80	3.10
			BS2-234	7	−248		1.65	1.76			1.98	2.61	3.51
e1h1n1													
N	HIP	3/2	BS-15	125	160		1.69	1.72					1.44
NH	HID		BS-15	59	−18		1.81	1.72			1.70	3.10	
	HIE		BS-15	0	0		1.81	1.73			1.65	2.92	2.98
e2h2n1													
NH	HIP	1	BS7-235	130	172		1.80	1.74			1.68		1.63
NH_2	HID		BS7-235	55	54		1.95	1.91			1.76	3.08	
	HIE		BS7-235	0	3		1.96	1.92			1.76		2.91
			BS-16	27	0		1.94	1.96			1.78		2.97
e3h3n1													
NH_2	HIP	½	BS10-147	50	83		1.97	2.09			1.75	1.93	
NH_3	HID		BS10-147	5	19		2.08	2.33			1.60	1.83	
	HIE		BS10-147	0	31		2.18	2.21			1.58	2.60	2.87
			BS2-234	6	0		2.24	2.12			1.52	2.74	2.96
e0	HID	3/2	BS10-147	41	39						2.08[a]		
	HIE		BS10-147	0	0						2.17[a]		3.03

[a] Gln-191 proton on OE1 is the donor.
[b] Gln-191 OE1 distance to Fe6.

In conclusion, our best N_2-bound E_4 state involves end-on NNH_2 with HIE (cf. Fig. 3) and strongly favourable protonation of N_2.

3.2. E_5 structures with N_2H_3

Next, we added an electron and a proton and studied the various $e_3h_3n_2$ structures. Adding a proton to the side-on HNNH structure, gives the side-on $HNNH_2$ structure, shown in Fig. 4 (bottom left; HIE state). It has a somewhat longer Fe2–N bond for the doubly protonated N atom than the HNNH structure, 1.98 Å, whereas the Fe6–N bond is slightly shorter, 1.78 Å. The N–N bond length is 1.41 Å. There is still a hydrogen bond between the ligand and the carbonyl of Gln-191 (1.58 Å). We studied this complex in both the triplet and the quintet states and the two states were essentially degenerate (within 2 kJ/mol with both basis sets). For the triplet, BS7-247 was lowest in energy, whereas for the quintet, BS-17

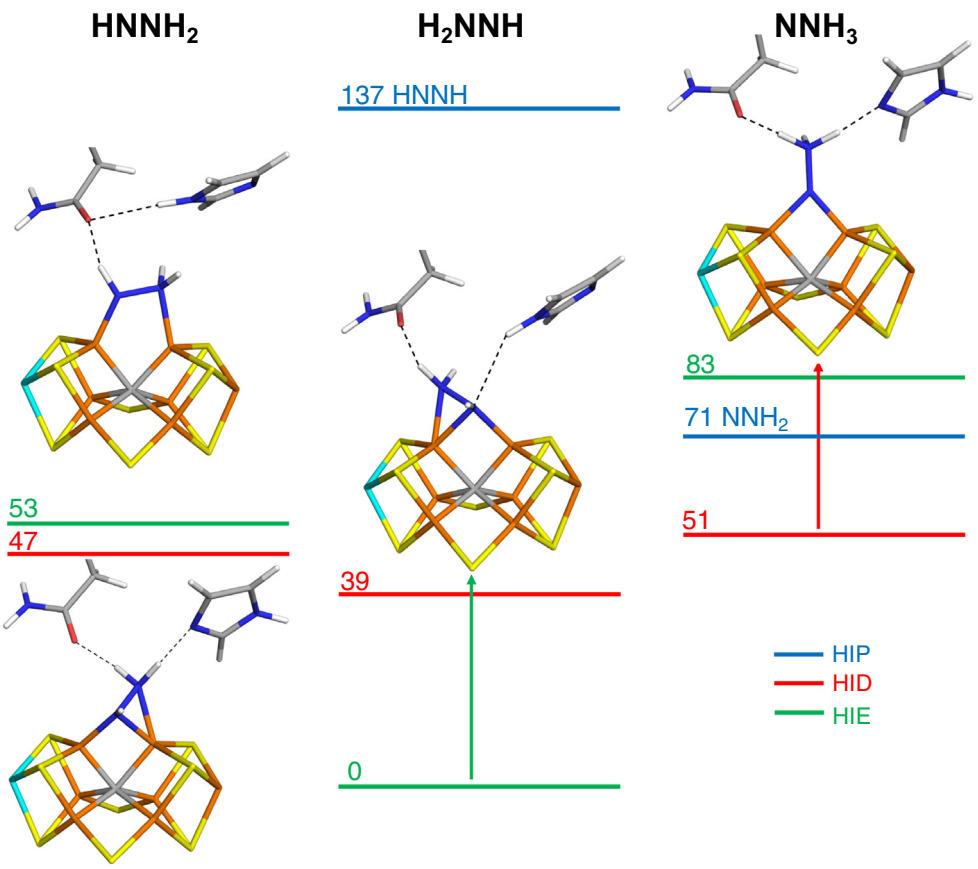

Fig. 4. The QM/MM geometries and TPSS/def2-SV(P) energies (kJ/mol) of the E_5 structures with $HNNH_2$, H_2NNH and NNH_3.

(only two Fe ions with negative spin) was found to be lowest in energy (but BS7-247 was only 4 kJ/mol less stable). The spin densities are similar to those of the HNNH complex and there is no spin density on the $HNNH_2$ ligand.

A slightly (6 kJ/mol) more stable structure can be obtained with the opposite protonation of His-195 (HID structure, also shown in Fig. 4). It involves a mixture of end-on and side-on binding with the singly protonated N atom bridging Fe2 and Fe6 with Fe–N distances of 1.89 and 1.88 Å, whereas the doubly protonated N atom is 2.00 Å from Fe2. The two protons of the NH_2 group form hydrogen bonds to Gln-191 and His-195, 1.70 and 1.68 Å, respectively.

However, the most stable structure is obtained by protonating the other N atom of HNNH (the one closes to Gln-191). This gives the structure in the centre of Fig. 4 (HIE state) and it has a similar asymmetrical coordination with Fe2–N = 1.95 Å, Fe6–N = 2.00 Å for the singly protonated N atom and Fe6–N = 1.93 Å for the doubly protonated N atom. It has a short hydrogen bond between the NH_2 group and Gln-191 (1.54 Å). His-195 also points towards the NH group with a H···N distance of 2.62 Å. It is 53 kJ/mol more stable than the other HIE–$HNNH_2$ structure. The corresponding HID structure has Fe2–N = Fe6–N = 1.92 Å for the singly protonated N atom and Fe6–N = 1.96 Å for the other N atom, $H\cdots O^{E1}$ = 1.53 Å and $H\cdots N^{E2}$ = 3.37 Å (opposite polarity), but it is 39 kJ/mol less stable than the HIE structure (55 kJ/mol with B3LYP) but 8 kJ/mol more stable than the HID–$HNNH_2$ structure.

The end-on NNH_3 complex was most stable in the quintet state. It has still an intact N–N bond of 1.40 Å (HIE state). The two Fe–N bonds are almost unchanged compared to the NNH_2 structure (1.78 and 1.81 Å). It has a strong hydrogen bond to Gln-191 (1.38 Å). In fact, when His-195 is instead protonated on the ND1 atom, the NNH_3 complex is stabilised by 32 kJ/mol, owing to a favourable hydrogen bond between one of the protons on NNH_3 and His-195 (1.66 Å; shown in the right side of Fig. 4). However, in contrast to the situation for the E_4 intermediates, the end-on NNH_3 structure turned out to be less stable than the best H_2NNH structure by 51–83 kJ/mol (34–78 kJ/mol with B3LYP). This is in contrast to the study by Nørskov et al. [20], which suggested a NNH_3 intermediate.

Interestingly, the dissociation of NH_3 from the NNH_3 intermediate is not automatic. The energy for the dissociation reaction (assuming that NH_3 ends up in the water solvent and that the N atom remains bound to the cluster in the e_0n_1 state) is highly unfavourable in the HID state (170 kJ/mol). In the HIE state, it is still unfavourable by 47 kJ/mol, but this is close to the expected gain in translational and rotational entropy from the released NH_3. However, if the cluster is protonated (on His-195, without any addition of an electron, i.e. an $e_3h_4n_2$ state), the dissociation becomes favourable by 48 kJ/mol and if an electron is also added ($e_4h_4n_2$, i.e. a E_6 state), the reaction is even more favourable, 78 kJ/mol.

The N_2H_3 structures are appreciably more stable than the corresponding N_2H_2 structures with a protonated His-195: The HIP–HNNH structure is 137 kJ/mol less stable than the HIE–H_2NNH structure and the HIP–NNH_2 structure automatically reorganises to the HID–NNH_3 structure. This shows that protonation of the N_2H_2 ligand is strongly favourable.

In conclusion, our calculations indicate that the most stable E_5 state is HIE–H_2NNH, i.e. indicating an alternating reaction mechanism, in contrast to the suggestions by Nørskov and coworkers [20]. Moreover, we show that the preferred binding mode is a mixture between end-on and side-on binding (cf. Fig. 4).

3.3. E_6 ($e_4h_4n_2$) structures with N_2H_4

As already mentioned, we can obtain the HIP–NNH_3 structure, from which NH_3 can dissociate with a reaction energy of –78 kJ/mol. In fact, we can also find an end-on $HNNH_3$ complex with an intact N–N bond of 1.45 Å and two Fe–N bonds of 1.91 Å (HIE state). It has a very short hydrogen bond to Gln-191 (1.40 Å). It is most stable in the singlet BS10-147 state. The corresponding HID structure is similar (Fig. 5, right side; Fe–N = 1.94 and 1.92 Å; H···OE1 = 1.45 Å). In fact, it is 33 kJ/mol more stable than the HIE structure (36 kJ/mol with B3LYP), because it is stabilised by the hydrogen bond to His-195 (1.64 Å). From the HIE–$HNNH_3$ structure, the reaction energy for the dissociation of NH_3 is almost thermoneutral (+1 kJ/mol), so that the reaction is expected to be favourable if the reaction entropy is included. However, from the HID complex, the dissociation is strongly unfavourable (by 93 kJ/mol).

Moreover, we can also obtain a structure with a cleaved N–N bond, one N bound to the cluster and NH_4^+ hydrogen bonded to it (1.54 Å). The latter group forms also hydrogen bonds to Gln-191 and His-195 (both 1.62 Å; HID structure). It was 64 kJ/mol less stable than the $HNNH_3$ structure.

However, all these structures are less stable than structures in which H_2NNH_2 (i.e. hydrazine) binds side-on to the cluster. With HIE, it has a N–N bond length of 1.45 Å and the Fe–N bonds are 1.96 and 1.98 Å (Fig. 5, left side). It has a strong hydrogen bond between H_2NNH_2 and Gln-191 (1.54 Å), but His-195 also forms a hydrogen bond to the OE1 atom of Gln-191 (2.24 Å). The structure is most stable in the BS10-135 state (but several other BS states are close in energy). It has low spin populations on both the Fe2 and Fe6 ions (1.7 and 1.4). This structure is 13–46 kJ/mol more stable than the $HNNH_3$ structures (78–114 kJ/mol with B3LYP).

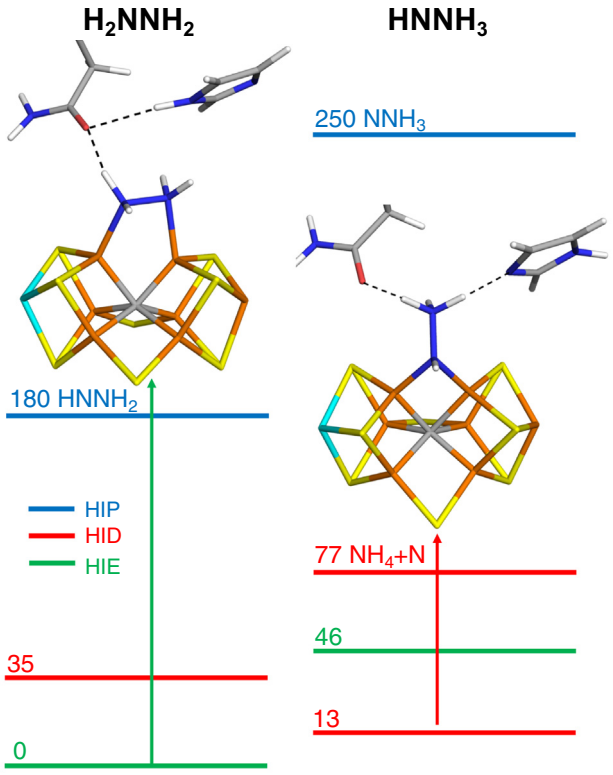

Fig. 5. The QM/MM geometries and TPSS/def2-SV(P) energies (kJ/mol) of the E_6 structures with H_2NNH_2 or $HNNH_3$.

The corresponding HID–H_2NNH_2 structure has a similar geometry, with Fe–N bonds of 1.97 and 1.98 Å. H_2NNH_2 forms hydrogen bonds to both Gln-191 (1.50 Å) and His-195 (1.72 Å). Still, it is 35 (83) kJ/mol less stable than the HIE structure, reflecting that intrinsically HIE is more stable than HID. The corresponding HIP–H_2NNH and HIP–$HNNH_2$ structures are 139 and 180 kJ/mol less stable than the best HIE–H_2NNH_2 structure (189 and 233 kJ/mol with B3LYP), again showing that protonation of the N_2H_3 ligand is favourable.

In conclusion, our results indicate that the HIE–H_2NNH_2 hydrazine complex is the most stable E_6 state, still supporting an alternating mechanism.

3.4. E_7 structures with N_2H_5

Next, we study the E_7 states. When adding an extra electron and proton to the H_2NNH_2 structure, a H_2NNH_3 structure can be formed. It has an intact N–N bond of 1.46 Å, but the triply protonated N atom has dissociated from Fe2, whereas the other N atom still binds to Fe2 (Fe–N = 1.99 Å; left side of Fig. 6; HID state). It is stabilised by hydrogen bonds both to Gln-191 (1.63 Å) and His-195 (1.56 Å).

However, it is strongly favourable to cleave the N–N bond, forming a NH_2 + NH_3 complex (it can be done with an activation barrier of only 31 kJ/mol). In the HIE structure (Fig. 6, centre), the NH_2 group bridges Fe2 and Fe6 with Fe–N distances of 1.96 and 1.87 Å, whereas NH_3 binds terminally to Fe2 with a Fe–N distance of 2.05 Å. NH_2 forms a hydrogen bond to the OE1 atom of Gln-191 with a H···O distance of 1.71 Å. The HE2 atom of His-195 also forms a hydrogen bond to the OE1 atom with a distance of 2.15 Å. The singlet and triplet states were close in energy (4 kJ/mol). The former is most stable in the BS10-135 state, whereas the latter is more stable in the BS6-157 and BS7-235 states.

The corresponding HID complex is similar, with Fe–N bonds of 1.85, 1.99 and 2.07 Å. However, the hydrogen bond between NH_2 and the side-chain OE1 atom of Gln-191 is slightly shorter 1.66 Å. In addition, it has a hydrogen bond between NH_3 and the NE2 atom of His-195, but it is long, 2.09 Å, and with a suboptimal geometry. This structure is 101 kJ/mol less stable than the HIE structure with both TPSS and B3LYP. The corresponding HIP–H_2NNH_2 structure is 196 kJ/mol less stable and therefore 297 kJ/mol less stable than the HIE–NH_2 + NH_3 structure, again illustrating the strongly favourable protonation of the ligand. We have also found a HIE structure with NH_3 on Fe6 and NH_2 bridging Fe2 and Fe6. It was 23 kJ/mol higher in energy than the best HIE structure. A similar structure in which NH_2 binds only to Fe2, but with a hydrogen bond from NH_3 to NH_2 (1.74 Å) is 100 kJ/mol less stable than the best HIE structure (both structures are shown in the right-hand side of Fig. 6.

As for the NNH_3 structure, the reaction energy for the dissociation of NH_3 from the HIENH_2 + NH_3 complex is unfavourable by 105 kJ/mol. However, if another electron and proton are added, this energy goes down to 21 kJ/mol, which could be overcome by entropic effects from the released NH_3 molecule. In fact, NH_3 can be released from Fe6 in this complex with a small barrier (14 kJ/mol) and a favourable reaction energy (16 kJ/mol; giving NH_3 hydrogen bonding to Cys-275, S1A and S2A).

3.5. E_5–E_8 structures with a single N atom

Finally, we studied structures with only one N atom bound. To make the study complete, we included also the E_5–E_6 states, even if our results favour an alternating mechanism (which involves a single N atom only in the E_7 and E_8 states, cf. Fig. 2). The structure of the N^{3-} complex (E_5; e_0n_1) is shown in Fig. 7 (left side; HIE state). It can be seen that N is symmetrically coordinated to both Fe2 and Fe6 with both Fe–N distances equal to 1.70 Å. The N atom is

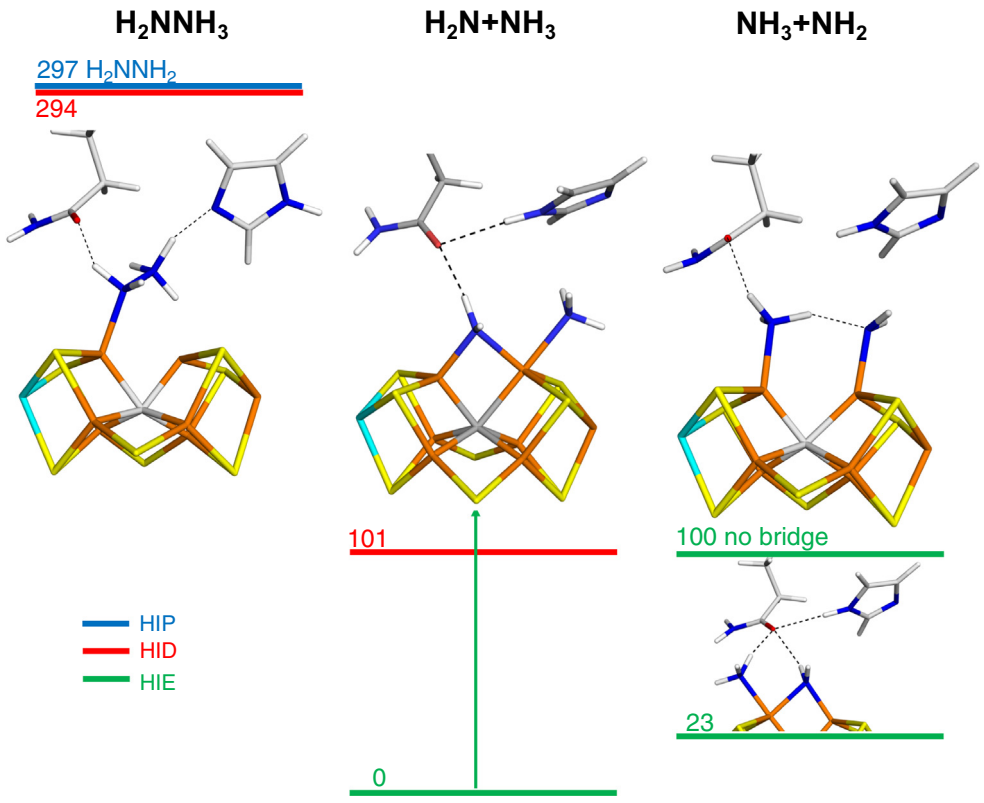

Fig. 6. The QM/MM geometries and TPSS/def2-SV(P) energies (kJ/mol) of the E_7 structures with N_2H_5.

2.80 Å from HE2 of His-195. It is most stable in the quintet state with only two negative spins on Fe1 and Fe5, i.e. the BS-15 state. It has a very small spin population on Fe6 (0.7) and rather low populations also on Fe2 (1.9) and Fe7 (2.0). The HID structure is similar, with Fe–N bonds of 1.69 and 1.71 Å. It is not stabilised by any hydrogen bonds and it is therefore 86 kJ/mol less stable than the HIE complex (85 kJ/mol with B3LYP).

Adding a proton and an electron to these structures gives the NH^{2-} E_6 state ($e_1h_1n_1$; Fig. 7 with HIE). The NH ligand still binds to both Fe2 and Fe6 with Fe–N distances of 1.81 and 1.73 Å. NH

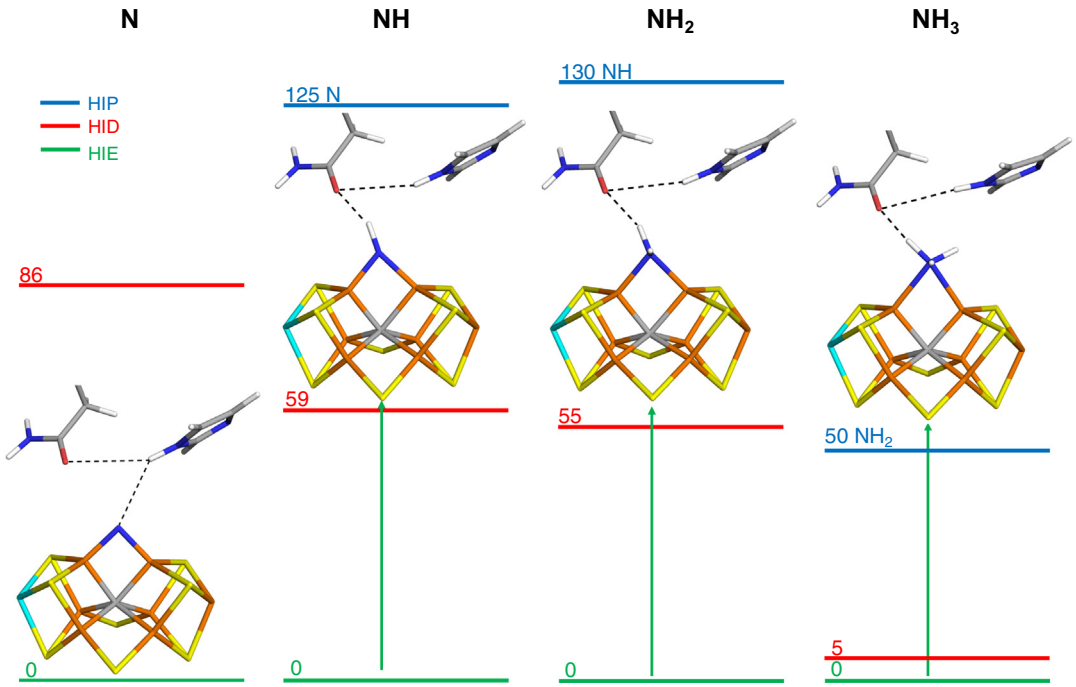

Fig. 7. The QM/MM geometries and TPSS/def2-SV(P) energies (kJ/mol) of the E_5–E_8 structures with a single N atom, i.e. with N^{3-}, NH^{2-}, NH_2^- and NH_3. Note that the energies in the four parts of the figure are not comparable.

forms a hydrogen bond to Gln-191 (1.65 Å). It was found to be most stable in the quartet state with two negative spins on Fe1 and Fe5 (BS-15). The spin population on Fe6 is still very low, 0.4. The corresponding HID structure has also Fe–N distances of 1.81 and 1.72 Å. The hydrogen-bond distance is 1.70 Å. NE2 of His-195 is 3.10 Å from the hydrogen atom of NH. It is 59 kJ/mol less stable than the HIE complex with TPSS, but actually 18 kJ/mol more stable with B3LYP. The corresponding HIP–N complex is 125 kJ/mol less stable than the HIE complex (160 kJ/mol with B3LYP), showing that protonation of N^{3-} is favourable.

Adding another electron and proton to the NH complex, gives the E_7 NH_2^- complex ($e_2h_2n_1$), which is also shown in Fig. 7 (with HIE). The ligand is still bound to both Fe ions with Fe–N bonds of 1.92 and 1.96 Å. NH_2 forms a hydrogen bond to Gln-191 (1.76 Å). The structure is most stable in the triplet state (BS7-235), but the quintet state is close in energy (4 kJ/mol less stable). Fe6 has a rather low spin population (1.6), whereas Fe2 has a normal spin population (–2.8) compared to the other Fe ions (2.3–3.2). The corresponding HID complex is similar, with Fe–N bonds of 1.91 and 1.95 Å and the same hydrogen-bond length. It is 55 kJ/mol less stable than the HIE structure, but it is 75 kJ/mol more favourable than the HIP–NH structure (54 and 118 kJ/mol with B3LYP, respectively).

Next, we added the eighth electron and proton to the NH_2^- complex, giving a NH_3 complex (e_3h_3n). It is shown in the right-hand side of Fig. 7 (with HIE). NH_3 is still symmetrically bound to Fe2 and Fe6 with Fe–N distances of 2.18 and 2.21 Å. The hydrogen bond to Gln-191 is 1.58 Å. It was found to be most stable in the doublet state with BS10-147. The spin population on Fe2 (2.3) is only slightly smaller than that on the other Fe ions (2.5–3.2). The corresponding HID complex is similar, with Fe–N bonds of 2.08 and 2.33 Å, and a hydrogen-bond length of 1.60 Å. However, the NH_3 group forms a hydrogen bond also to His-195, 1.83 Å. Therefore, it is only 5 kJ/mol less stable than the HIE complex. It is 45 kJ/mol more stable than the HIP–NH_2^- complex (19 and 64 kJ/mol with B3LYP), i.e. protonation of NH_2^- is still downhill. This is the only complex in this section that is involved in our preferred alternating reaction path.

Finally, we tried to dissociate NH_3 from this E_8 state, which was not facile. The reaction energy for the dissociation of NH_3 was strongly unfavourable, by 160 and 195 kJ/mol for the HIE and HID structures, respectively. The dissociation energy of NH_3 was only partly improved if the complex was protonated (i.e. to the $e_3h_4n_1$ state), 150 kJ/mol. If it was also reduced ($e_4h_4n_1$), the reaction energy decreased to 111 kJ/mol, which is still too large. The problem is most likely that that the dissociation of NH_3 leaves Fe2 and Fe6 coordinatively unsaturated. Therefore, we investigated whether the reaction energies were improved if SH^- binds when NH_3 dissociates. We then assumed that SH^- comes from the pocket formed by the flip of Gln-191 and that Gln-191 rotates back to its original position when S2B rebinds (it gains 67 kJ/mol by that back-rotation in our calculations). Quite satisfactory, this changed the reaction energy for dissociation of NH_3, accompanied by the rebinding of SH^- to the cluster (giving the protonated e_0h_1 state) so that it became favourable by 153 and 177 kJ/mol for HIE and HID, respectively.

4. Conclusions

We have investigated putative reaction paths for N_2 replacing S2B in Mo-nitrogenase using QM/MM calculations, inspired by two recent crystal structures, showing that the S2B group may reversibly dissociate from the catalytic cluster [8,39]. We have studied all possible protonation states of the N_2-derived ligand and of His-19 5 for the E_4–E_8 intermediates. Based on these calculations, we suggest the reaction mechanism summarised in Fig. 8. The reaction starts with N_2 binding to the empty S2B site, between Fe2 and Fe6, in an irregular half-bridging mode. N_2 is then protonated by the two protons, already present in the cluster in the E_4 state. The first protonation is slightly upwards (17 kJ/mol), whereas the second protonation is strongly favourable by 148 kJ/mol. However, it should be noted that these energies are very uncertain, as we did not perform any full investigation of all (~2500) possible positions of the two protons in the FeMo cluster [43]. On the other hand, our calculations quite conclusively suggest that the most stable N_2H_2 structure has NNH_2 bound end-on with one N atom binding Fe2 and Fe6 (Fig. 3; rather than side-on binding HNNH).

For the E_5 state, many different structures are possible and we find that the H_2NNH structure in Fig. 4 is most stable. It shows an irregular structure with the singly protonated N atom bridging Fe2 and Fe6, whereas the doubly protonated N binds only to Fe6. For the E_6 state, a rather symmetric H_2NNH_2 (hydrazine) structure is most stable (Fig. 5). When it is reduced and protonated to the E_7 state, the N–N bond is easily cleaved, giving NH_2^- bridging Fe2 and Fe6, whereas NH_3 is bound to only Fe2 (Fig. 6). Finally, after the final reduction, NH_3 dissociates and NH_2^- is protonated to NH_3. The latter group cannot dissociate until S2B rebinds to the cluster.

In most of these structures, the protonated N_2-ligand forms hydrogen bonds to the OE2 atom of the rotated Gln-191 residue. The sidechain of His-195 is also close to the ligand and we have tested three possible protonation states of it, HID, HIE and HIP. In all cases, the HIP structure is strongly unfavourable and may easily protonate the ligand, suggesting a possible protonation path of the ligand. However, as has been discussed by Dance, [80] it is unlikely that His-195 may provide more than one proton to the substrate. It would also give the HID state after the proton transfer, whereas we find that the HIE state is preferred for all structures in the suggested reaction path.

Thus, we suggest a mechanism that is mainly alternating: For E_5–E_7, the protons are added alternatingly to the two N atoms. Moreover, the calculations suggest that hydrazine (H_2NNH_2) is a reaction intermediate and the first NH_3 product does not dissociate until the E_7 state. However, for the E_4 intermediate, we actually suggest that the NNH_2 structure, rather than HNNH, is most stable, although the former intermediate traditionally is connected to the distal reaction mechanism.

In the latter aspect, our calculations agree with those in the previous study by Nørskov and coworkers [20]. However, they then suggested a distal mechanism, forming NNH_3 after the addition of the third proton. Our calculations agree that such a mechanism is also possible. However, for the key E_5 state, we find that the H_2NNH intermediate is significantly more stable. It is likely that Nørskov did not consider all possible N_2H_3 intermediates and their QM-cluster model was quite small, excluding the crucial Gln-191 and His-195 residues. Therefore, we strongly believe that the present QM/MM results with a large QM system and the explicit consideration of the surrounding protein and solvent are more reliable than Nørskov's QM-cluster calculations with a minimal cluster model of the active site.

Kästner and Blöchl have suggested a mechanism of nitrogenase in which S5A only dissociated from Fe7 but remained bound to Fe3 [32,81]. The calculations were based on an incorrect model with a central nitride ion, without considering the formation of H_2 (N_2 binds to the E_2 state) and were performed on a minimal QM-cluster without any account of the surrounding. They suggested that N_2 binds bridging Fe3 and Fe7 after dissociation of the protonated S5A from Fe7 (but not from Fe3), and follows a mainly alternating mechanism. However, they suggested that HNNH and $HNNH_3$ are involved in the mechanism, rather than NNH_2 and H_2NNH_2 in our mechanism. Again, we believe that our calculations

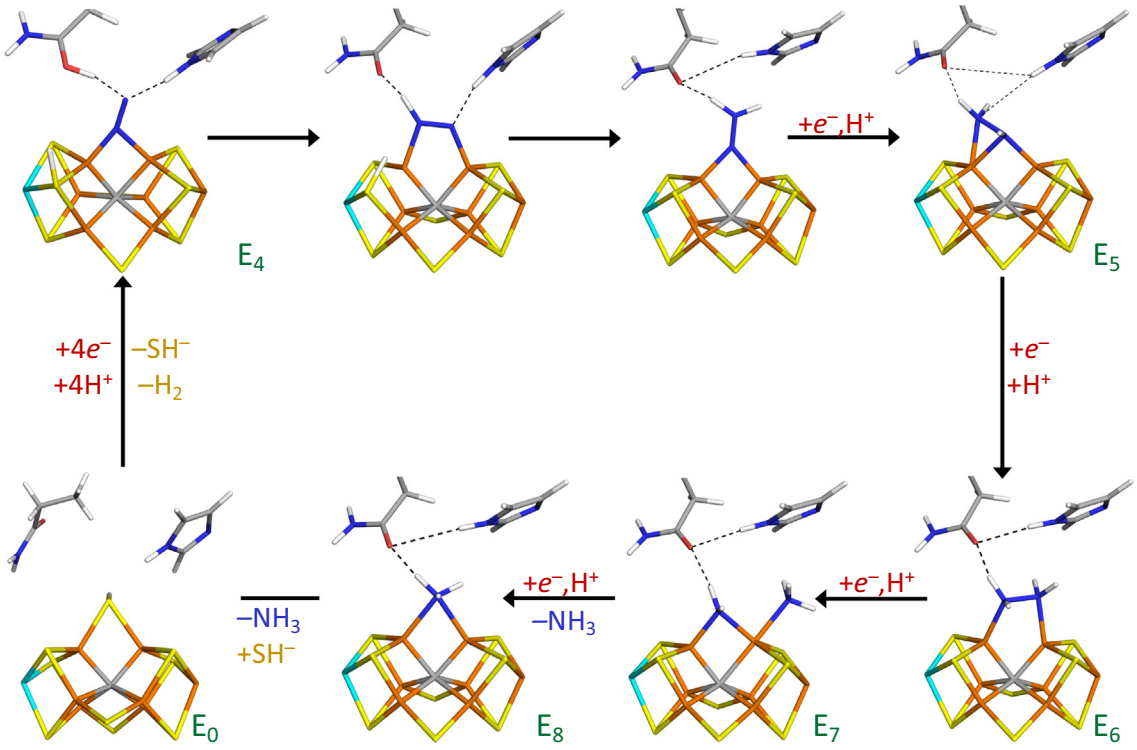

Fig. 8. Suggested reaction mechanism of Mo-nitrogenase with a dissociated S2B, based on the QM/MM calculations.

with a correct FeMo model and full account of the surroundings are more accurate.

Recently, we have considered possible structures for N_2H_2 binding to the intact FeMo cluster (i.e. with S2B still bound and Gln-191 in the non-flipped orientation) [48]. The calculations still indicated that Fe2 and Fe6 are the most probable binding sites for N_2H_2. However, the most stable structure had *trans*-HNNH bound terminally to Fe2. This is in contrast to the present result, where end-on bound NNH_2 is most stable. Structures involving NNH_2 were also tested for the intact cluster, but they were found to be at least 28 kJ/mol less stable than the best structure. However, a structure with $HNNH_2$ bound to Fe6, where the third proton was transferred automatically from the homocitrate ligand, was quite low in energy, 3–29 kJ/mol less stable than the best structure.

In conclusion, we have shown that Mo-nitrogenase may bind N_2 in the empty site formed by dissociation of the S2B ligand and this molecule can then be reduced and protonated to two molecules of ammonia along a favourable alternating mechanism, which is 51 kJ/mol more favourable than a distal mechanism at the E_5 intermediate. However, this does of course not prove that this is the actual mechanism followed by Mo-nitrogenase. To that end, similar studies are needed for the corresponding reaction without dissociation of S2B (or with S2B dissociated from only one of Fe2 or Fe6 as has recently been suggested both computationally and experimentally [79,82,83]), as well as detailed studies of the dissociation mechanism and the binding of N_2. These will be investigated in future studies.

Declaration of Competing Interest

The authors declared that there is no conflict of interest.

Acknowledgements

This investigation has been supported by grants from the Swedish research council (projects 2018-05003), from COST, European union through Action CM1305 (ECOSTBio), from China Scholarship Council, from eSSENCE: the e-science collaboration and from the Royal Physiographic Society in Lund. The computations were performed on computer resources provided by the Swedish National Infrastructure for Computing (SNIC) at Lunarc at Lund University and HPC2N at Umeå University.

Appendix A. Supplementary data

Supplementary data to this article can be found online at https://doi.org/10.1016/j.jcat.2020.08.028.

References

[1] B.K. Burgess, D.J. Lowe, Mechanism of Molybdenum Nitrogenase, Chem. Rev. 96 (1996) 2983–3012, https://doi.org/10.1021/cr950055x.
[2] B. Schmid, H.-J. Chiu, V. Ramakrishnan, J.B. Howard, D.C. Rees, Nitrogenase. In *Handbook of Metalloproteins*, John Wiley & Sons Ltd (2006) 1025–1036, https://doi.org/10.1002/0470028637.met174.
[3] B.M. Hoffman, D. Lukoyanov, Z.-Y. Yang, D.R. Dean, L.C. Seefeldt, Mechanism of Nitrogen Fixation by Nitrogenase: The Next Stage, Chem. Rev. 114 (2014) 4041–4062, https://doi.org/10.1021/cr400641x.
[4] B.E. Smith, Nitrogenase Reveals Its Inner Secrets, Science (80) 297 (2002) 1654–1655.
[5] J. Kim, D.C. Rees, Structural Models for the Metal Centers in the Nitrogenase Molybdenum-Iron Protein, Science (80) 257 (5077) (1992) 1677–1682, https://doi.org/10.1126/science.1529354.
[6] O. Einsle, F.A. Tezcan, S.L.A. Andrade, B. Schmid, M. Yoshida, J.B. Howard, D.C. Rees, Nitrogenase MoFe-Protein at 1.16 Å Resolution: A Central Ligand in the FeMo-Cofactor, Science (80) 297 (5587) (2002) 1696, https://doi.org/10.1126/science.1073877.
[7] Spatzal, T.; Aksoyoglu, M.; Zhang, L.; Andrade, S. L. A.; Schleicher, E.; Weber, S.; Rees, D. C.; Einsle, O. Evidence for Interstitial Carbon in Nitrogenase FeMo Cofactor. Science (80-.). 2011, 334, 940–940. https://doi.org/10.1126/science.1214025.
[8] T. Spatzal, K.A. Perez, O. Einsle, J.B. Howard, D.C. Rees, Ligand Binding to the FeMo-Cofactor: Structures of CO-Bound and Reactivated Nitrogenase, Science (80) 345 (6204) (2014) 1620–1623, https://doi.org/10.1126/science.1256679.
[9] O. Einsle, Nitrogenase FeMo Cofactor: An Atomic Structure in Three Simple Steps, J. Biol. Inorg. Chem. 19 (6) (2014) 737–745, https://doi.org/10.1007/s00775-014-1116-7.
[10] R.R. Eady, Structure–Function Relationships of Alternative Nitrogenases, Chem. Rev. 96 (1996) 3013–3030, https://doi.org/10.1021/cr950057h.

[11] Lancaster, K. M.; Roemelt, M.; Ettenhuber, P.; Hu, Y.; Ribbe, M. W.; Neese, F.; Bergmann, U.; DeBeer, S. X-Ray Emission Spectroscopy Evidences a Central Carbon in the Nitrogenase Iron-Molybdenum Cofactor. Science (80-.). 2011, 334, 974–977. https://doi.org/10.5061/dryad.6m0f6870.

[12] R. Bjornsson, F.A. Lima, T. Spatzal, T. Weyhermüller, P. Glatzel, E. Bill, O. Einsle, F. Neese, S. DeBeer, Identification of a Spin-Coupled Mo(III) in the Nitrogenase Iron-Molybdenum Cofactor, Chem. Sci. 5 (8) (2014) 3096–3103, https://doi.org/10.1039/C4SC00337C.

[13] R.Y. Igarashi, M. Laryukhin, P.C. Dos Santos, H.-I. Lee, D.R. Dean, L.C. Seefeldt, B. M. Hoffman, Trapping H^- Bound to the Nitrogenase FeMo-Cofactor Active Site during H_2 Evolution: Characterization by ENDOR Spectroscopy, J. Am. Chem. Soc. 127 (2005) 6231–6241, https://doi.org/10.1021/ja043596p.

[14] V. Hoeke, L. Tociu, D.A. Case, L.C. Seefeldt, S. Raugei, B.M. Hoffman, High-Resolution ENDOR Spectroscopy Combined with Quantum Chemical Calculations Reveals the Structure of Nitrogenase Janus Intermediate E4(4H), J. Am. Chem. Soc. 141 (2019) 11984–11996, https://doi.org/10.1021/jacs.9b04474.

[15] L.E. Roth, F.A. Tezcan, X-Ray Crystallography, Methods Mol. Biol. 766 (2011) 147–164, https://doi.org/10.1007/978-1-61779-194-9_10.

[16] C. Van Stappen, L. Decamps, G.E. Cutsail, R. Bjornsson, J.T. Henthorn, J.A. Birrell, S. DeBeer, The Spectroscopy of Nitrogenases, Chem. Rev. (2020) 120, https://doi.org/10.1021/acs.chemrev.9b00650. doi: 10.1021/acs.chemrev.9b00650.

[17] R.N.F. Thorneley, D.J. Lowe, Kinetics and Mechanism of the Nitrogenase Enzyme System, in: T.G. Spiro (Ed.), Molybdenum Enzymes, Wiley, New York, 1985, pp. 221–284.

[18] P.P. Hallmen, J. Kästner, N_2 Binding to the FeMo-Cofactor of Nitrogenase, Zeitschrift Anorg. Allg. Chemie 641 (1) (2015) 118–122, https://doi.org/10.1002/zaac.201400114.

[19] I. Dance, Activation of N_2, the Enzymatic Way, Zeitschrift Anorg. Allg. Chemie 641 (2015) 91–99, https://doi.org/10.1002/zaac.201400120.

[20] J.B. Varley, Y. Wang, K. Chan, F. Studt, J.K. Nørskov, Mechanistic Insights into Nitrogen Fixation by Nitrogenase Enzymes, PCCP 17 (44) (2015) 29541–29547, https://doi.org/10.1039/C5CP04034E.

[21] P.E.M. Siegbahn, Model calculations suggest that the central carbon in the FeMo-cofactor of nitrogenase becomes protonated in the process of nitrogen fixation, J. Am. Chem. Soc. 138 (33) (2016) 10485–10495, https://doi.org/10.1021/jacs.6b03846.

[22] M.L. McKee, A new nitrogenase mechanism using a CFe_8S_9 model: does H_2 elimination activate the complex to N_2 addition to the central carbon atom?, J Phys. Chem. A 120 (5) (2016) 754–764, https://doi.org/10.1021/acs.jpca.5b10384.

[23] L. Rao, X. Xu, C. Adamo, Theoretical investigation on the role of the central carbon atom and close protein environment on the nitrogen reduction in Mo nitrogenase, ACS Catal. 6 (3) (2016) 1567–1577, https://doi.org/10.1021/acscatal.5b02577.

[24] S. Raugei, L.C. Seefeldt, B.M. Hoffman, Critical computational analysis illuminates the reductive-elimination mechanism that activates nitrogenase for N_2 reduction, Proc. Natl. Acad. Sci. 115 (2018) 10521–10530, https://doi.org/10.1073/pnas.1810211115.

[25] I. Dance, Computational investigations of the chemical mechanism of the enzyme nitrogenase, ChemBioChem (2020), https://doi.org/10.1002/cbic.201900636. doi: 10.1002/cbic.201900636.

[26] F. Tuczek, Nitrogen Fixation in Nitrogenase and Related Small-Molecule Models: Results of DFT Calculations, in: R. Hille, C. Schulzke, M.L. Kirk (Eds.), RSC Metallobiology Series 7, Royal Society of Chemistry, Cambridge, 2017, pp. 223–274.

[27] I. Dance, Theoretical investigations of the mechanism of biological nitrogen fixation at the FeMo cluster site, J. Biol. Inorg. Chem. 1 (6) (1996) 581–586, https://doi.org/10.1007/s007750050096.

[28] K.K. Stavrev, M.C. Zerner, Studies on the hydrogenation steps of the nitrogen molecule at the Azotobacter vinelandii nitrogenase site, Int. J. Quantum Chem. 70 (6) (1998) 1159–1168.

[29] P.E.M. Siegbahn, J. Westerberg, M. Svensson, R.H. Crabtree, Nitrogen fixation by nitrogenases: a quantum chemical study, J. Phys. Chem. B 102 (9) (1998) 1615–1623, https://doi.org/10.1021/jp972207t.

[30] T. Lovell, J. Li, T. Liu, D.A. Case, L. Noodleman, FeMo cofactor of nitrogenase: a density functional study of states MN, Mox, MR, and MI, J. Am. Chem. Soc. 123 (2001) 12392–12410, https://doi.org/10.1021/ja011860y.

[31] H. Xie, R. Wu, Z. Zhou, Z. Cao, Exploring the interstitial atom in the femo cofactor of nitrogenase: insights from QM and QM/MM calculations, J. Phys. Chem. B 112 (36) (2008) 11435–11439, https://doi.org/10.1021/jp803616z.

[32] J. Kästner, P.E. Blöchl, Ammonia production at the FeMo cofactor of nitrogenase: results from density functional theory, J. Am. Chem. Soc. 129 (2007) 2998–3006, https://doi.org/10.1021/ja068618h.

[33] D. Lukoyanov, S.A. Dikanov, Z.-Y. Yang, B.M. Barney, R.I. Samoilova, K.V. Narasimhulu, D.R. Dean, L.C. Seefeldt, B.M. Hoffman, ENDOR/HYSCORE studies of the common intermediate trapped during nitrogenase reduction of N_2H_2, CH_3N_2H, and N_2H_4 support an alternating reaction pathway for N_2 reduction, J. Am. Chem. Soc. 133 (2011) 11655–11664, https://doi.org/10.1021/ja2036018.

[34] J. Chatt, Chemistry relevant to the biological fixation of nitrogen, Annu. Proc. Phytochem. Soc. Eur. 18 (1980) 1–18.

[35] J. Chatt, J.R. Dilworth, R.L. Richards, Recent advances in the chemistry of nitrogen fixation, Chem. Rev. 78 (1978) 589–625, https://doi.org/10.1021/cr60316a001.

[36] D.V. Yandulov, R.R. Schrock, Catalytic reduction of dinitrogen to ammonia at a single molybdenum center, Science (80) 301 (2003) 76–78, https://doi.org/10.1126/science.1085326.

[37] R.R. Schrock, Catalytic reduction of dinitrogen to ammonia at a single molybdenum center, Acc. Chem. Res. 38 (2005) 955–962, https://doi.org/10.1021/ar0501121.

[38] R.R. Schrock, Catalytic reduction of dinitrogen to ammonia by molybdenum: theory versus experiment, Angew. Chemie Int. Ed. 47 (2008) 5512–5522, https://doi.org/10.1002/anie.200705246.

[39] Sippel, D.; Rohde, M.; Netzer, J.; Trncik, C.; Gies, J.; Grunau, K.; Djurdjevic, I.; Decamps, L.; Andrade, S. L. A.; Einsle, O. A Bound Reaction Intermediate Sheds Light on the Mechanism of Nitrogenase. Science (80-.). 2018, 359 (6383), 1484–1489. https://doi.org/10.1126/science.aar2765.

[40] R.N.F. Thornely, R.R. Eady, D.J. Lowe, Biological nitrogen fixation by way of an enzyme-bound dinitrogen-hydride intermediate, Nature 272 (1978) 557–558, https://doi.org/10.1038/272557a0.

[41] R.N.F. Thorneley, D.J. Lowe, The mechanism of Klebsiella pneumoniae nitrogenase action. Pre-steady-state kinetics of an enzyme-bound intermediate in N_2 reduction and of NH_3 formation, Biochem. J. 224 (3) (1984) 887–894, https://doi.org/10.1042/bj2240887.

[42] B. Benediktsson, A.T. Thorhallsson, R. Bjornsson, QM/MM calculations reveal a bridging hydroxo group in a vanadium nitrogenase crystal structure, Chem. Commun. 54 (2018) 7310–7313, https://doi.org/10.1039/C8CC03793K.

[43] L. Cao, O. Caldararu, U. Ryde, Protonation and reduction of the FeMo cluster in nitrogenase studied by quantum mechanics/molecular mechanics (QM/MM) calculations, J. Chem. Theory Comput. 14 (2018) 6653–6678, https://doi.org/10.1021/acs.jctc.8b00778.

[44] L. Cao, O. Caldararu, U. Ryde, Protonation states of homocitrate and nearby residues in nitrogenase studied by computational methods and quantum refinement, J. Phys. Chem. B 121 (2017) 8242–8262, https://doi.org/10.1021/acs.jpcb.7b02714.

[45] L. Cao, U. Ryde, Influence of the protein and DFT method on the broken-symmetry and spin states in nitrogenase, Int. J. Quantum Chem. 118 (2018), https://doi.org/10.1002/qua.25627.

[46] L. Cao, U. Ryde, What is the structure of the E_4 state in nitrogenase?, J. Chem. Theory Comput. 16 (2020) 1936–1952, https://doi.org/10.1021/acs.jctc.9b01254.

[47] L. Cao, U. Ryde, Extremely large differences in DFT energies for nitrogenase models, Phys. Chem. Chem. Phys. 21 (2019) 2480–2488, https://doi.org/10.1039/C9CP06930A.

[48] L. Cao, U. Ryde, N_2H_2 binding to the nitrogenase FeMo cluster, studied by QM/MM methods, J. Biol. Inorg. Chem. 25 (2020) 521–540, https://doi.org/10.1007/s00775-020-01780-5.

[49] R. Bjornsson, F. Neese, S. DeBeer, Revisiting the Mössbauer isomer shifts of the FeMoco cluster of nitrogenase and the cofactor charge, Inorg. Chem. 56 (3) (2017) 1470–1477, https://doi.org/10.1021/acs.inorgchem.6b02540.

[50] B.M. Barney, J. Mcclead, D. Lukoyanov, M. Laryukhin, T. Yang, D.R. Dean, B.M. Hoffman, L.C. Seefeldt, Diazene (HN=NH) Is a substrate for nitrogenase : insights into the pathway of N_2 reduction, Biochemistry 46 (2007) 6784–6794.

[51] D.A. Case, J.T. Berryman, R.M. Betz, D.S. Cerutti, T.E. Cheatham, T.A. Darden, R.E. Duke, T.J. Giese, H. Gohlke, A.W. Goetz, et al., AMBER 14, University of California, San Francisco, 2014.

[52] J.A. Maier, C. Martinez, K. Kasavajhala, L. Wickstrom, K.E. Hauser, C. Simmerling, FF14SB: improving the accuracy of protein side chain and backbone parameters from FF99SB, J. Chem. Theory Comput. 11 (2015) 3696–3713, https://doi.org/10.1021/acs.jctc.5b00255.

[53] W.L. Jorgensen, J. Chandrasekhar, J.D. Madura, R.W. Impey, M.L. Klein, Comparison of simple potential functions for simulating liquid water, J. Chem. Phys. 79 (2) (1983) 926–935, https://doi.org/10.1063/1.445869.

[54] L. Hu, U. Ryde, Comparison of methods to obtain force-field parameters for metal sites, J. Chem. Theory Comput. 7 (8) (2011) 2452–2463, https://doi.org/10.1021/ct100725a.

[55] J. Tao, J.P. Perdew, V.N. Staroverov, G.E. Scuseria, Climbing the density functional ladder: non-empirical meta-generalized gradient approximation designed for molecules and solids 146401 Phys. Rev. Lett. 91 (14) (2003), https://doi.org/10.1103/PhysRevLett.91.146401.

[56] A. Schäfer, H. Horn, R. Ahlrichs, Fully optimized contracted gaussian basis sets for atoms Li to Kr, J. Chem. Phys. 97 (4) (1992) 2571–2577, https://doi.org/10.1063/1.463096.

[57] B.H. Besler, K.M. Merz, P.A. Kollman, Atomic charges derived from semiempirical methods, J. Comput. Chem. 11 (4) (1990) 431–439, https://doi.org/10.1002/jcc.540110404.

[58] F. Furche, R. Ahlrichs, C. Hättig, W. Klopper, M. Sierka, F. Weigend, Turbomole, Wiley Interdiscip. Rev. Comput. Mol. Sci. 4 (2) (2014) 91–100, https://doi.org/10.1002/wcms.1162.

[59] A.D. Becke, Density-functional exchange-energy approximation with correct asymptotic-behavior, Phys. Rev. A 38 (6) (1988) 3098–3100, https://doi.org/10.1103/PhysRevA.38.3098.

[60] C. Lee, W. Yang, R.G. Parr, Development of the Colle–Salvetti correlation-energy formula into a functional of the electron density, Phys. Rev. B 37 (2) (1988) 785–789.

[61] A.D. Becke, A new mixing of hartree-fock and local density-functional theories, J. Chem. Phys. 98 (2) (1993) 1372, https://doi.org/10.1063/1.464304.

[62] K. Eichkorn, O. Treutler, H. Öhm, M. Häser, R. Ahlrichs, Auxiliary basis-sets to approximate Coulomb potentials, Chem. Phys. Lett. 240 (4) (1995) 283–289, https://doi.org/10.1016/0009-2614(95)00621-a.

[63] K. Eichkorn, F. Weigend, O. Treutler, R. Ahlrichs, Auxiliary basis sets for main row atoms and transition metals and their use to approximate Coulomb potentials, Theor. Chem. Acc. 97 (1–4) (1997) 119–124, https://doi.org/10.1007/s002140050244.
[64] S. Grimme, J. Antony, S. Ehrlich, H. Krieg, A consistent and accurate ab initio parametrization of density functional dispersion correction (DFT-D) for the 94 elements H-Pu, J. Chem. Phys. 132 (15) (2010), https://doi.org/10.1063/1.3382344.
[65] S. Grimme, S. Ehrlich, L. Goerigk, Effect of the damping function in dispersion corrected density functional theory, J. Comput. Chem. 32 (7) (2011) 1456–1465, https://doi.org/10.1002/jcc.21759.
[66] C. Greco, P. Fantucci, U. Ryde, L. de Gioia, Fast generation of broken-symmetry states in a large system including multiple iron-sulfur assemblies: investigation of QM/MM energies, clusters charges, and spin populations, Int. J. Quantum Chem. 111 (2011) 3949–3960, https://doi.org/10.1002/qua.22849.
[67] R.K. Szilagyi, M.A. Winslow, On the accuracy of density functional theory for iron−sulfur clusters, J. Comput. Chem. 27 (12) (2006) 1385–1397, https://doi.org/10.1002/jcc.20449.
[68] U. Ryde, The coordination of the catalytic zinc in alcohol dehydrogenase studied by combined quantum-chemical and molecular mechanics calculations, J. Comput. Aided Mol. Des. 10 (1996) 153–164.
[69] U. Ryde, M.H.M. Olsson, Structure, strain, and reorganization energy of blue copper models in the protein, Int. J. Quantum Chem. 81 (2001) 335–347.
[70] N. Reuter, A. Dejaegere, B. Maigret, M. Karplus, Frontier bonds in QM/MM methods: a comparison of different approaches, J. Phys. Chem. A 104 (2000) 1720–1735, https://doi.org/10.1021/jp9924124.
[71] L. Hu, P. Söderhjelm, U. Ryde, On the convergence of QM/MM energies, J. Chem. Theory Comput. 7 (2011) 761–777, https://doi.org/10.1021/ct100530r.
[72] L. Cao, U. Ryde, On the difference between additive and subtractive QM/MM calculations, Front. Chem. 6 (2018) 89, https://doi.org/10.3389/fchem.2018.00089.
[73] D. Lukoyanov, N. Khadka, Z.-Y. Yang, D.R. Dean, L.C. Seefeldt, B.M. Hoffman, Reductive elimination of H_2 activates nitrogenase to reduce the N≡N triple bond: characterization of the E_4(4H) Janus intermediate in wild-type enzyme, J. Am. Chem. Soc. 138 (2016) 10674–10683, https://doi.org/10.1021/jacs.6b06362.
[74] P.E.M. Siegbahn, Is there computational support for an unprotonated carbon in the E_4 state of nitrogenase?, J. Comput. Chem. 39 (2018) 743–747, https://doi.org/10.1002/jcc.25145.
[75] P.E.M. Siegbahn, The mechanism for nitrogenase including all steps, Phys. Chem. Chem. Phys. 21 (2019) 15747–15759, https://doi.org/10.1039/c9cp02073j.
[76] I. Dance, Survey of the geometric and electronic structures of the key hydrogenated forms of FeMo-Co, the active site of the enzyme nitrogenase: principles of the mechanistically significant coordination chemistry, Inorganics 7 (2019), https://doi.org/10.3390/inorganics7010008.
[77] T. Spatzal, J. Schlesier, E.-M. Burger, D. Sippel, L. Zhang, S.L.A. Andrade, D.C. Rees, O. Einsle, Nitrogenase FeMoco investigated by spatially resolved anomalous dispersion refinement, Nat. Commun. 7 (2016) 10902, https://doi.org/10.1038/ncomms10902.
[78] M. Rohde, D. Sippel, C. Trncik, S.L.A. Andrade, O. Einsle, The critical E_4 state of nitrogenase catalysis, Biochemistry 57 (2018) 5497–5504, https://doi.org/10.1021/acs.biochem.8b00509.
[79] A.T. Thorhallsson, B. Benediktsson, R. Bjornsson, A model for dinitrogen binding in the E_4 state of nitrogenase, Chem. Sci. 10 (2019) 11110–11124, https://doi.org/10.1039/C9SC03610E.
[80] I. Dance, The hydrogen chemistry of the FeMo-Co active site of nitrogenase, J. Am. Chem. Soc. 127 (2005) 10925–10942, https://doi.org/10.1021/ja0504946.
[81] J. Kästner, P.E. Blöchl, Towards an understanding of the workings of nitrogenase from DFT calculations, ChemPhysChem 6 (2005) 1724–1726, https://doi.org/10.1002/cphc.200400474.
[82] I. Dance, How Feasible Is the Reversible S-Dissociation Mechanism for the Activation of FeMo-Co{,} the Catalytic Site of Nitrogenase?, Dalt. Trans. 48 (2019) 1251–1262, https://doi.org/10.1039/C8DT04531C.
[83] D.A. Lukoyanov, M.D. Krzyaniak, D.R. Dean, M.R. Wasielewski, L.C. Seefeldt, B. M. Hoffman, Time-resolved EPR study of H_2 reductive elimination from the photoexcited nitrogenase Janus E_4(4H) intermediate, J. Phys. Chem. B 123 (2019) 8823–8828, https://doi.org/10.1021/acs.jpcb.9b07776.